第 44 卷 第 7 期/2024 年 4 月/光学学报 研究论文

光学学报

基于石墨烯的全光纤主动锁模激光器

苏友朋[1,2]，常建华[1,2,3*]，陆天一[1,2]，崔志远[1,2]，涂倩[1,2]，朱云瀚[1,2]

[1]南京信息工程大学天长研究院，安徽 滁州 239300；

[2]南京信息工程大学电子与信息工程学院，江苏 南京 210044；

[3]南京信息工程大学江苏省大气环境与装备技术协同创新中心，江苏 南京 210044

摘要 利用光纤倏逝波耦合效应，设计了一种基于石墨烯全光纤结构的主动锁模激光器。该石墨烯全光纤锁模器件基于侧面腐蚀的单模光纤，构建了银/聚二甲基硅氧烷(PDMS)/石墨烯的电容型结构，腐蚀的单模光纤置于PDMS和石墨烯之间。实验结果显示，在电容结构两端施加与激光腔的共振频率一致及其整数倍的周期性方波电压信号，并对腔内光进行调制，可实现1558 nm光纤激光器的主动锁模。所设计的主动锁模激光器获得了基本频率及二次谐波的锁模脉冲，重复频率分别为12.2 MHz和24.4 MHz，实现了电控重复频率的脉冲输出。这种石墨烯全光纤锁模器件具有低成本、低功耗的优势，为实现灵活可控的主动锁模激光器提供了新思路。

关键词 激光器；光纤激光器；石墨烯；全光纤结构；主动锁模

中图分类号 TN25 **文献标志码** A **DOI**：10.3788/AOS231958

1 引 言

超快脉冲光纤激光器由于其结构紧凑、光束质量高等优势[1]，被广泛应用于光纤通信[2]、医学[3]、精密材料加工[4]等领域。锁模技术是实现超短脉冲的一种有效方法[5]，主动锁模激光器通过在激光腔内引入主动调制器件，利用外部调制信号改变光信号的特性，实现激光器锁模脉冲输出[6-7]，具有灵活可控、输出脉冲稳定的优势[8]。然而，此类调制器通常尺寸较大、价格昂贵且波长调制范围受限，例如铌酸锂调制器，增加了激光器的成本和复杂性[9]。为了实现简单灵活可集成化的主动锁模脉冲激光器，研究微型、低成本、低功耗的电光调制器具有重要意义。

近年来，石墨烯由于其优异的电光性能而得到广泛研究[10]，其光学特性受化学势(费米能级)的影响，研究表明，通过外加电场可改变石墨烯的费米能级，实现对光吸收的调控。因此，基于石墨烯的电光调制器具备实现主动锁模激光器的潜力。2020年，Kovalchuk等[11]利用制作的石墨烯/聚甲基丙烯酸甲酯(PMMA)/石墨烯电容器件作为光纤激光器的锁模开关，通过在电容器两端施加偏置电压使石墨烯的费米能级发生变化，从而改变石墨烯的非线性光吸收，降低石墨烯的饱和吸收功率，实现连续波(CW)到锁模(CWML)的切换。2022年，Dai等[12]基于优化电极结构和绝缘层的石墨烯电光调制器，以较低的调制功率对石墨烯的非线性传输进行调控，降低了饱和损耗，在Nd∶YVO_4全固态激光器上演示了电开关操作，实现了调Q、调Q锁模(QML)和连续波锁模(CWML)之间的模式切换。上述锁模激光器利用偏置电压对石墨烯的费米能级进行静态调控，实现可切换的模式运转，其本质依然是基于石墨烯的可饱和吸收特性，属于被动式锁模。相比于主动锁模，被动锁模往往需要更高泵浦功率以达到饱和吸收体的饱和吸收光强，且激光器重复频率不可调控。因此，2018年，Bogusławski等[13]利用制备的石墨烯反射式电光器件实现了1560 nm光纤激光器的基频及二次谐波主动锁模，通过施加在器件两端的交流信号动态改变石墨烯的吸收，利用交流电压信号控制锁模脉冲信号的产生。此基于石墨烯的电光调制器可以很好地响应电压信号，实现激光器可控重复频率的主动锁模操作，相比外加调制器实现主动锁模具有小型化、低成本等优势。然而，石墨烯反射式电光器件存在一些局限。首先，石墨烯对光的吸收能力有限，这导致其在光调制时的效率相对较低。其次，石墨烯的损伤阈值较低，这限制了它在高功率激光器中的使用。此外，石墨烯反射式电光器件在实际应用中还需要特殊的固定方法，难以实现激光器的集成。

因此，本文基于石墨烯高载流子迁移率的特性，利用腐蚀的单模光纤产生的倏逝波增加光与石墨烯的相

收稿日期：2023-12-21；**修回日期**：2024-01-12；**录用日期**：2024-01-23；**网络首发日期**：2024-02-20

基金项目：国家自然科学基金(62175114，62375137)

通信作者：*jianhuachang@nuist.edu.cn

互作用长度，构造了一种高效、高速的全光纤石墨烯电容型器件，该器件以较低的调制功耗实现了石墨烯光学性能的高速调控，同时具有较高的调制效率。将该器件应用于环形光纤激光系统，调制信号频率为激光腔共振频率（12.2 MHz）及其整数倍，在调制信号的控制下，周期性地改变石墨烯对腔内光的吸收，进而调整和控制激光在腔内的增益，使其满足共振条件。在一定的泵浦功率下，成功实现了1558 nm光纤激光器的基频与二次谐波的主动锁模操作。这种基于石墨烯的全光纤结构具有体积小、成本低、响应速率高和易于集成等优势，有利于主动锁模激光器的应用与发展。

2　实验装置及原理分析

2.1　器件制备及实验装置

石墨烯全光纤锁模器件的结构图及截面图如图1(a)、(b)所示，由石墨烯、单模光纤、聚二甲基硅氧烷（PDMS）、银（Ag）膜构成电容型结构（GCD）。选用玻璃作为基底，在玻璃上利用磁控溅射工艺镀50 nm的银作为底部电极，银具有较好的导电性，有利于降低器件的电阻。利用旋涂机在银层上旋涂一层200 nm厚的PDMS作为绝缘层，较薄的绝缘层能够有效降低其电容值。利用质量分数为20%的氢氟酸（HF）将标准单模光纤直径腐蚀至15 μm[14]，腐蚀长度为5 mm，将腐蚀后的单模光纤转移至PDMS上，为了提升绝缘层PDMS的亲水性，将器件放置于紫外臭氧清洗机（CCI UV250-MC，上海众频科技有限公司）处理10 min。石墨烯选用质量浓度为0.1 mg/mL的石墨烯分散液（XFZ20分散，南京先丰纳米材料科技公司）[15]，将石墨烯分散液滴涂至器件上，烘干后利用微电子打印机（MP1100，上海幂方电子科技有限公司）在器件上喷墨打印一层银电极层，最终将制作好的GCD器件利用银线接入电路板进行测试。

图1(c)为石墨烯表征的拉曼光谱，从图中可以观察到两个典型拉曼振动峰分别位于1350.15 cm^{-1}和1585.89 cm^{-1}处，符合石墨烯的拉曼光谱特征，二者分别代表石墨烯的D峰和G峰。其中D峰相对于石墨烯有所增强，其原因是使用的石墨烯溶液中存在部分氧原子杂质[16]。使用扫描电子显微镜（SEM）对石墨烯分散液的表面形貌进行了探测，如图1(d)所示，石墨烯纳米片呈大尺寸片状且具有良好的连续性[17]，有利于提高GCD器件的调制效果。

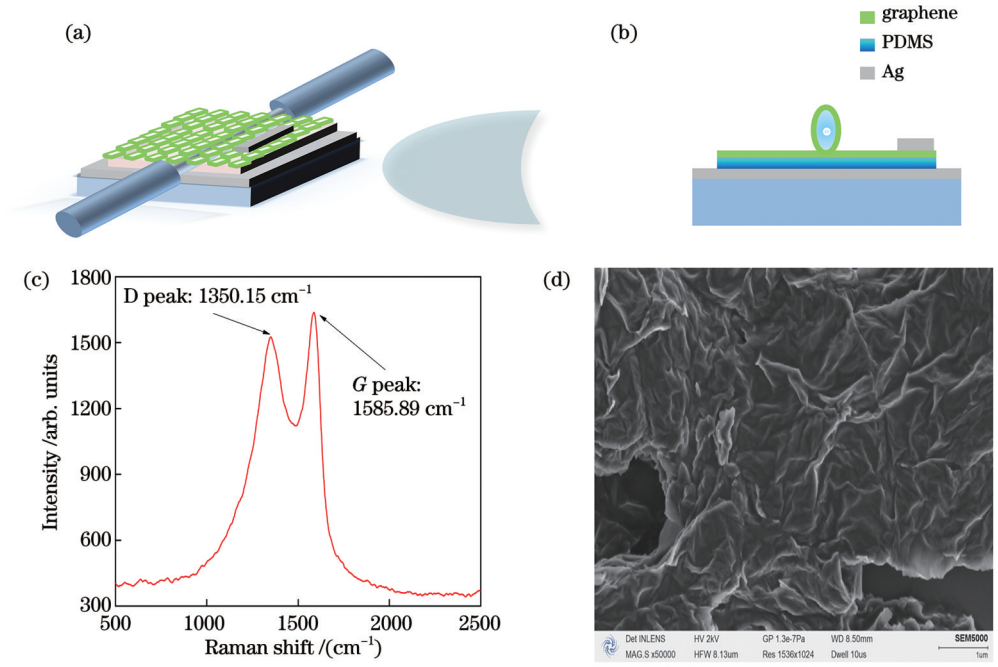

图1　GCD器件结构及石墨烯表征图。(a)GCD器件示意图；(b)GCD器件截面图；(c)石墨烯拉曼光谱；(d)石墨烯的扫描电子显微镜（SEM）图

Fig. 1　GCD device structure and graphene characterization. (a) Schematic diagram of GCD device; (b) side view of GCD device; (c) graphene Raman spectrum; (d) scanning electron microscope (SEM) image of graphene

图2所示为实验采用的1550 nm环形锁模激光系统示意图，所设计的激光器由一个980 nm激光二极管（CM97-750-76PM）作为泵浦源、一段5 m长的掺铒光纤、一个980 nm/1550 nm的波分复用器（WDM）、一个1550 nm的单向隔离器（ISO）、一个三环式偏振控制器（PC）和一个90∶10的输出耦合器组成。首先，980 nm的泵浦源将入射光经过WDM输入到激光腔中，经过掺铒光纤产生的1550 nm的增益光经过ISO，ISO用于确保增益光的单向传输，同时确保980 nm的泵浦光不会对实验产生影响，PC用于调整输出的偏振状态，最

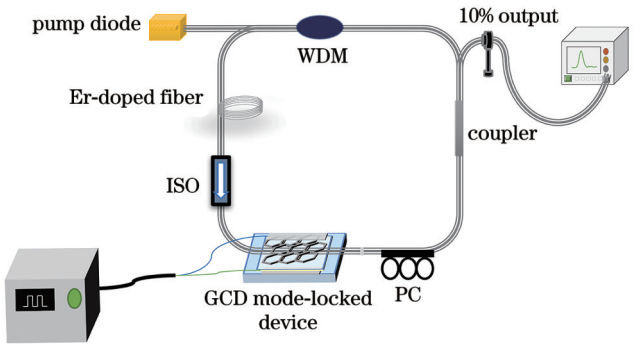

图 2 基于GCD器件的主动锁模激光系统

Fig. 2 Actively mode-locked laser system based on GCD devices

后将光以10%的比例输出用于测试，激光腔总腔长为16.8 m，对应于12.2 MHz的激光腔共振频率。将制备的GCD器件放置于隔离器和偏振控制器之间，测试系统利用光谱分析仪、数字示波器、功率计、自相关仪和频谱分析仪来记录锁模脉冲信号，包括光谱、脉冲宽度、重复频率和输出功率。

2.2 调制原理分析

石墨烯以其本身的零带隙结构表现出优异的光学吸收特性[18]，其吸收特性主要受化学势（费米能级）控制[19]，纯净的石墨烯费米能级位于狄拉克点处，如图3(a)所示，此时石墨烯内的自由电子需要较少的能量就可以从价带跃迁到导带。当对石墨烯调制器施加驱动电压时，调制器两端存在电位差，使石墨烯的内部载流子浓度发生变化，其内部载流子浓度与石墨烯的费米能级有关[20]，表达式为

$$n_s=\frac{2}{\pi\hbar^2 v_f^2}\int_0^{\infty}\varepsilon\left[f_d(\varepsilon)-f_d(\varepsilon+2\mu_c)\right]\mathrm{d}\varepsilon, \quad (1)$$

式中：$\hbar$是普朗克常量，约为6.582×10^{-16} eV·s/rad；v_f为费米速度；ε是载流子能量；μ_c是石墨烯的费米能级；$f_d(\varepsilon)=\left[\exp\left(\frac{\varepsilon-\mu_c}{K_BT}\right)+1\right]^{-1}$为费米-狄拉克分布，$K_BT$为玻尔兹曼常数。而石墨烯的费米能级在外加电压下会发生偏移，其费米能级与外加电压的关系[21]定义为

$$\mu_c=\hbar v_f\sqrt{a_0\pi|V+V_0|}, \quad (2)$$

式中：V为外加电压；a_0为在电压作用下材料层间的平板电容常数；V_0为石墨烯初始的化学势导致的补偿电压。而石墨烯的光学吸收系数[22]定义为

$$T=T^*\left[f_1(1-f_2)-f_2(1-f_1)\right]=T^*(f_1-f_2), \quad (3)$$

式中：T^*为初始吸收系数；f_1和f_2分别是载流子在价带和导带的费米占据概率。因此，在偏置电压的驱动下，石墨烯内部载流子浓度发生变化，这种变化会影响石墨烯的费米能级，从而改变石墨烯对光的吸收。

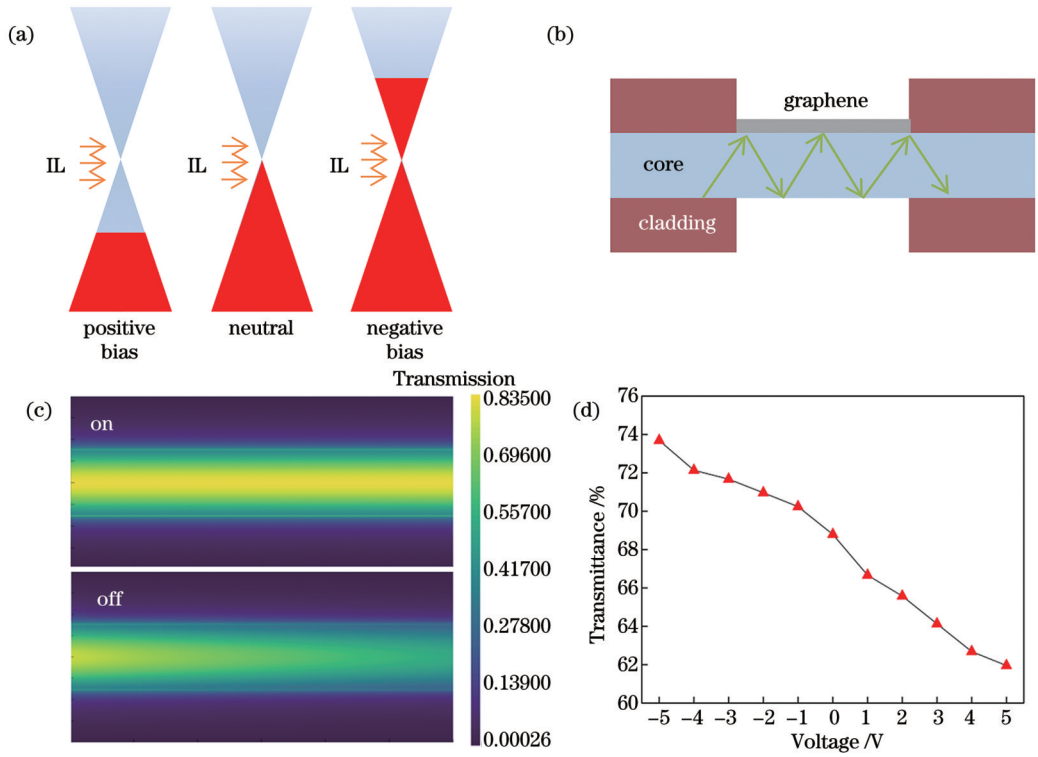

图 3 石墨烯器件的调制原理及传输效率。(a)石墨烯的吸收与费米能级的关系；(b)倏逝波耦合效应原理图；(c)5 V（上图）和0 V（下图）偏置电压下石墨烯覆盖的腐蚀光纤内部的光传输特性；(d)80 mW下光传输效率与电压幅值的关系

Fig. 3 Modulation principle and transmission efficiency of graphene modulator. (a) Relationship between absorption of graphene and Fermi level; (b) principle diagram of evanescent wave coupling effect; (c) optical transmission characteristics inside corroded fiber covered with graphene under bias voltages of 5 V (as shown in the figure above) and 0 V (as shown in the figure below); (d) relationship between optical transmission efficiency and voltage amplitude at 80 mW

本文所设计的石墨烯全光纤锁模器件基于光纤光波导和电容型结构，纤芯内部的光和石墨烯发生全反射，在介质边界附近形成倏逝光[23]，倏逝光和石墨烯产生吸收，改变了纤芯内部的光场强度，倏逝光增加了光和石墨烯的相互作用长度，能够有效地提高石墨烯器件的调制效率，如图 3(b)所示。利用FDTD对石墨烯覆盖的腐蚀光纤内部的光传输特性进行了仿真验证，如图 3(c)所示，当无电场作用时，传输光在石墨烯的吸收下表现出较大的损耗，当施加外加电场改变石墨烯的费米能级时，石墨烯的吸收性能降低，导致光纤内光场强度增强，实现了可调控的吸收性能。同时，石墨烯具有高载流子迁移率，使得平板电容型结构能够实现较高的调制速率，通过对电容型结构的导电层和绝缘层参数进行优化，有效减小器件的RC常数，使其能够响应较高的调制速率，实现费米能级的动态调控[24]。这种动态调控意味着石墨烯器件能够以调制信号的速率对光纤内部的光传输特性进行调制，而不依赖于石墨烯材料本身的饱和吸收特性，实现特定频率的光信号输出。因此，通过对石墨烯器件施加与激光腔共振频率一致的交流调制信号，周期性地改变石墨烯对激光腔内光的吸收性能，最终产生激光器的主动锁模脉冲信号。

为了更好地表征所设计石墨烯器件的调制效率，测试了制备的石墨烯器件在－5～5 V的偏置电压信号下的光传输特性，其传输效率随着偏置电压的增大从73.6%下降至62%，如图 3(d)所示。结果表明，在外加电场的作用下，石墨烯的费米能级发生偏移，在反向电压的驱动下，石墨烯的吸收有所增强，在正向偏压下，石墨烯的吸收有所减弱。传输效率的变化趋势代表石墨烯材料在制备过程中引入了掺杂，导致石墨烯的狄拉克点发生偏移，其呈现出P型半导体的特性。

3 实验结果与讨论

将GCD器件接入光纤激光系统，利用功率计(Thorlabs PM200)测量并记录了GCD器件的平均输出功率与泵浦功率之间的关系，如图 4(a)所示。随着泵浦功率的增大，激光器的平均输出功率与泵浦功率呈良好的线性关系。从图 4(a)可以看出：泵浦功率为20 mW时产生CW信号，为了获得较为明显的实验现象并保证石墨烯不会因过高的光功率密度而损毁，主动锁模实验的泵浦功率固定为80 mW，此时激光器的平均输出功率为1.328 mW。GCD器件依靠电压信号对石墨烯的吸收性能进行有效的调控，从而改变激光腔内的光场强度，实现对激光器输出性能的控制。图 4(b)显示了交流信号幅值的变化对其输出功率产生的影响。随着交流信号幅值的增大，石墨烯的费米能级在更大范围内被调控，导致平均输出功率呈下降趋势。在80 mW的泵浦功率下，将交流信号幅值从0 V增加到5 V，平均输出功率从1.328 mW下降至1.130 mW，经计算得出器件的插入损耗从1.54 dB增加到2.09 dB。信号幅值的增大提高了GCD器件的调控范围，导致器件的损耗增大，这与石墨烯器件在－5～5 V时的传输效率相吻合。

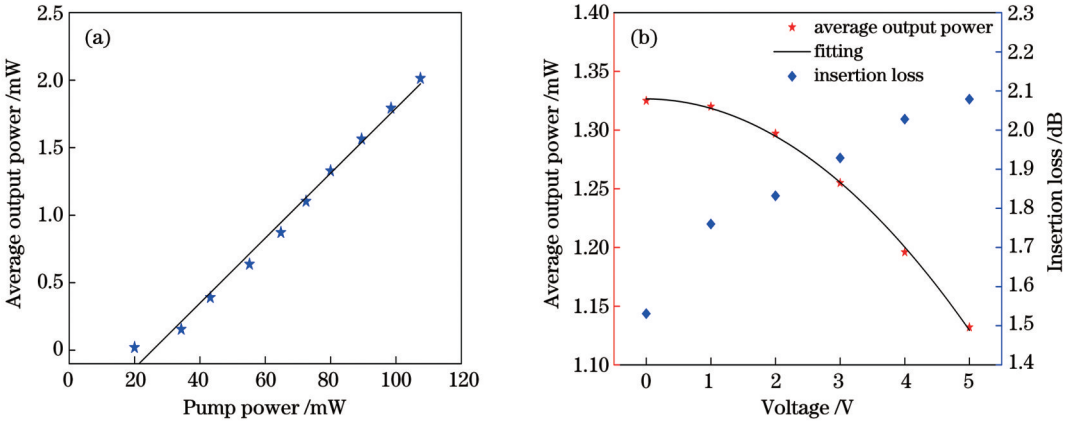

图4 光纤激光器的输出功率。(a)平均输出功率与泵浦功率的关系；(b)平均输出功率及插入损耗随电压的变化

Fig. 4 Output power of fiber laser. (a) Relationship between average output power and pump power; (b) variations of average output power and insertion loss with voltage

保持泵浦功率为80 mW，产生的输出信号由快速光电二极管(Newport 818-BB-21)和数字示波器(Agilent MSO7052B)记录，如图 5(a)、(b)所示。利用信号发生器(RIGOL DG1032)对石墨烯器件施加与激光腔共振频率一致的周期性交流信号(12.2 MHz)，当外加电压幅值为0 V时，示波器呈现出杂乱的连续波，代表此时激光腔内的光场强度未达到石墨烯的饱和吸收功率，激光器输出连续激光信号。随后增大电压幅值至1 V，利用石墨烯器件周期性地调整激光在激光腔内的增益，使输出信号呈现出有规律的脉冲波形，但由于电压幅值较低，器件对石墨烯费米能级的调控有限，导致石墨烯吸收的动态变化范围有限，因此观察到

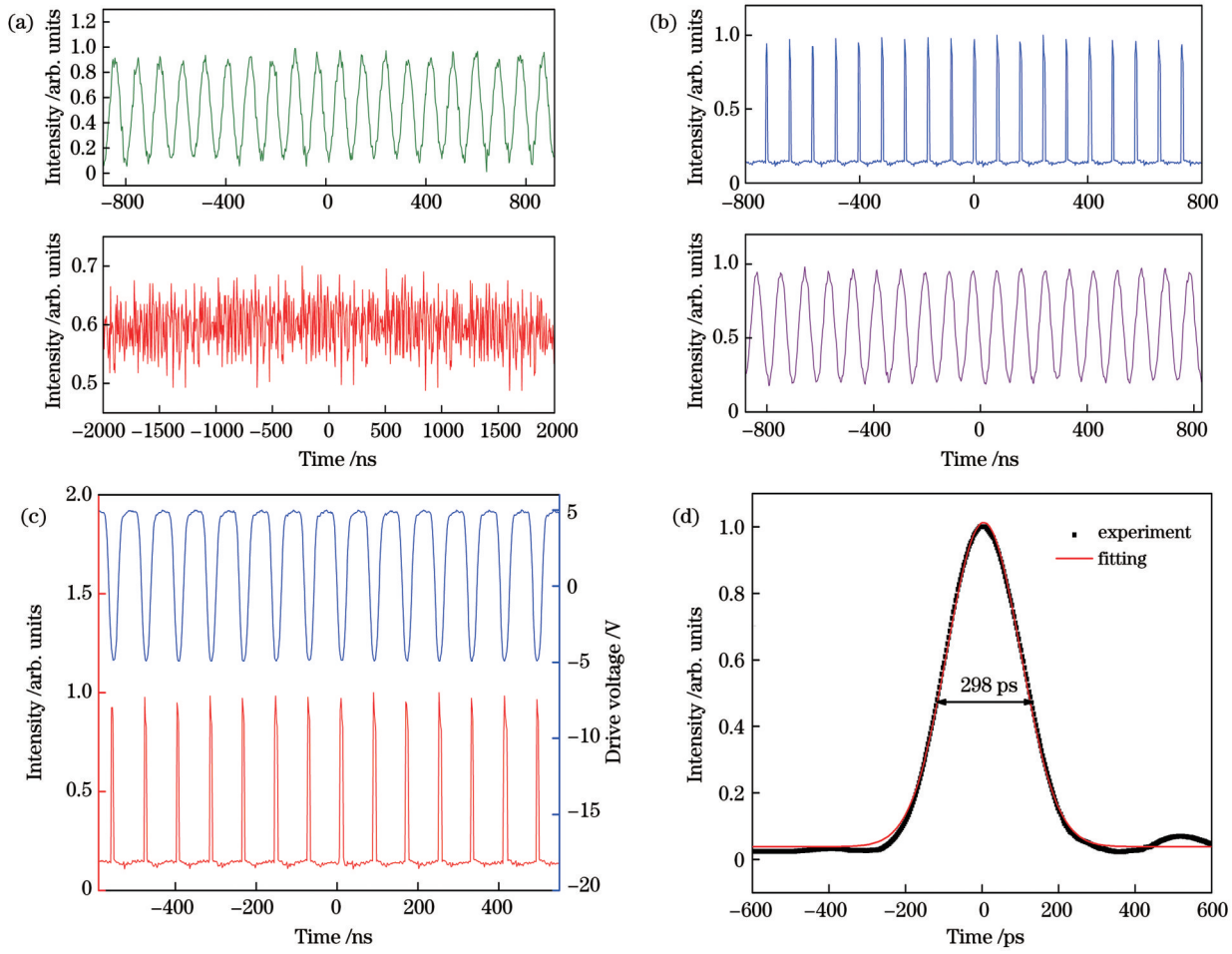

图 5　80 mW 泵浦功率下不同调制信号的脉冲序列示意图。(a) 1 V、3 V 交流电压信号下的脉冲序列图；(b)连续波与 5 V 交流(AC)信号下的锁模脉冲序列；(c)驱动电压信号与脉冲序列的同步图；(d)自相关曲线图

Fig. 5　Schematic diagrams of pulse sequence under different demodulation signals at 80 mW pump power. (a) Pulse sequence diagrams under 1 V and 3 V AC voltage signals; (b) mode locked pulse sequences under continuous wave and 5 V AC signal; (c) synchronous diagram of driving voltage signal and pulse sequence; (d) autocorrelation curves

不稳定的锁模脉冲信号[25]。继续增大电压幅值至 3 V，此时输出脉冲信号的稳定性得到显著提高。当将电压幅值加到 5 V 时，可观察到最稳定的脉冲信号，重复频率为 12.2 MHz，实现了激光器的主动锁模。将电压幅值在 0 V、5 V 之间进行切换，观察到 CW 到 CWML 的可逆切换，具有较高的稳定性。图 5(c)展示了脉冲波形与施加电信号的对比，脉冲的重复频率与电信号的频率保持良好的一致性，且 −5 V 对应脉冲的峰值，这与器件的传输效率吻合，表明 GCD 器件能够很好地响应调制信号。此时，利用商业自相关仪(FR-103HP)测量得到的自相关曲线如图 5(d)所示，测量结果显示，GCD 器件锁模的最窄脉冲宽度为 298 ps，锁模脉冲宽度的大小受石墨烯器件的响应速率影响；此外，激光器本身的色散效应会影响不同频率的光信号传输，进而对锁模信号的脉冲宽度产生影响。

为了测试搭建的激光系统的输出稳定性，在泵浦功率为 80 mW、交流信号为 ±5 V(12.2 MHz)下，利用分辨率为 0.25 nm 的光谱分析仪(Anritsu MS9740A)测量了激光系统的输出光谱，如图 6(a)所示。测量结果显示光纤激光器输出的激光中心波长为 1558 nm，半峰全宽(FWHM)为 0.6 nm。使用频谱仪(ESAd402B)测量了锁模光纤激光器的基频曲线，如图 6(b)所示，测量结果显示锁模信号的重复频率为 12.2 MHz，与调制信号一致，其射频信号的信噪比高达 58 dB，表明基于 GCD 器件的光纤锁模激光器稳定性良好。

主动锁模激光器的优势在于能够实现可控重复频率的脉冲激光输出，对于连续波，它的频率分量是连续分布的，通过石墨烯器件对两倍共振频率的光信号进行调制，可实现更高重复频率的谐波锁模脉冲[26]。实验中保持泵浦功率不变，将调制频率增加为激光腔共振频率的两倍(24.4 MHz)，腔内光信号在石墨烯器件的调控下发生倍频振荡，从而产生了谐波锁模操作，如图 7(a)所示。锁模脉冲信号略显不稳定，这可能是因为在更高的调制速率下，石墨

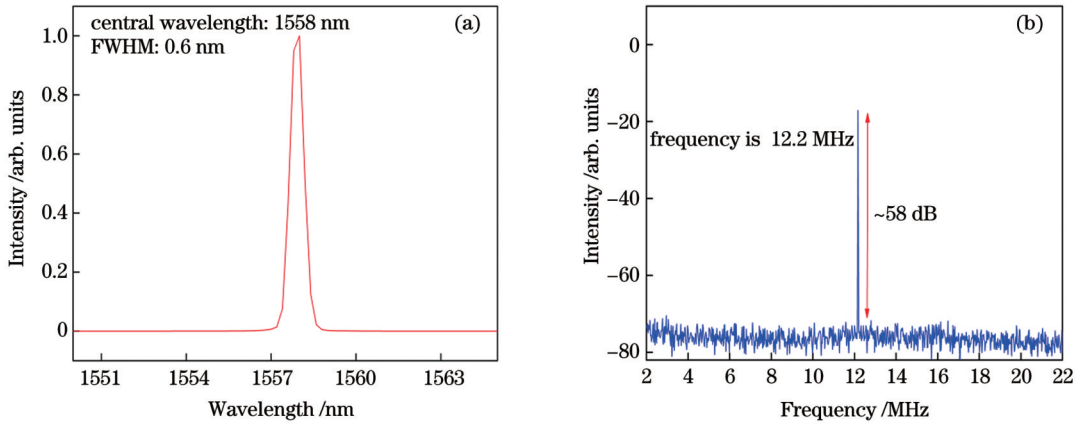

图 6　光纤激光器的输出特性。(a)光谱图;(b)频谱图

Fig. 6　Output characteristics of fiber laser. (a) Spectrogram; (b) frequency spectrum

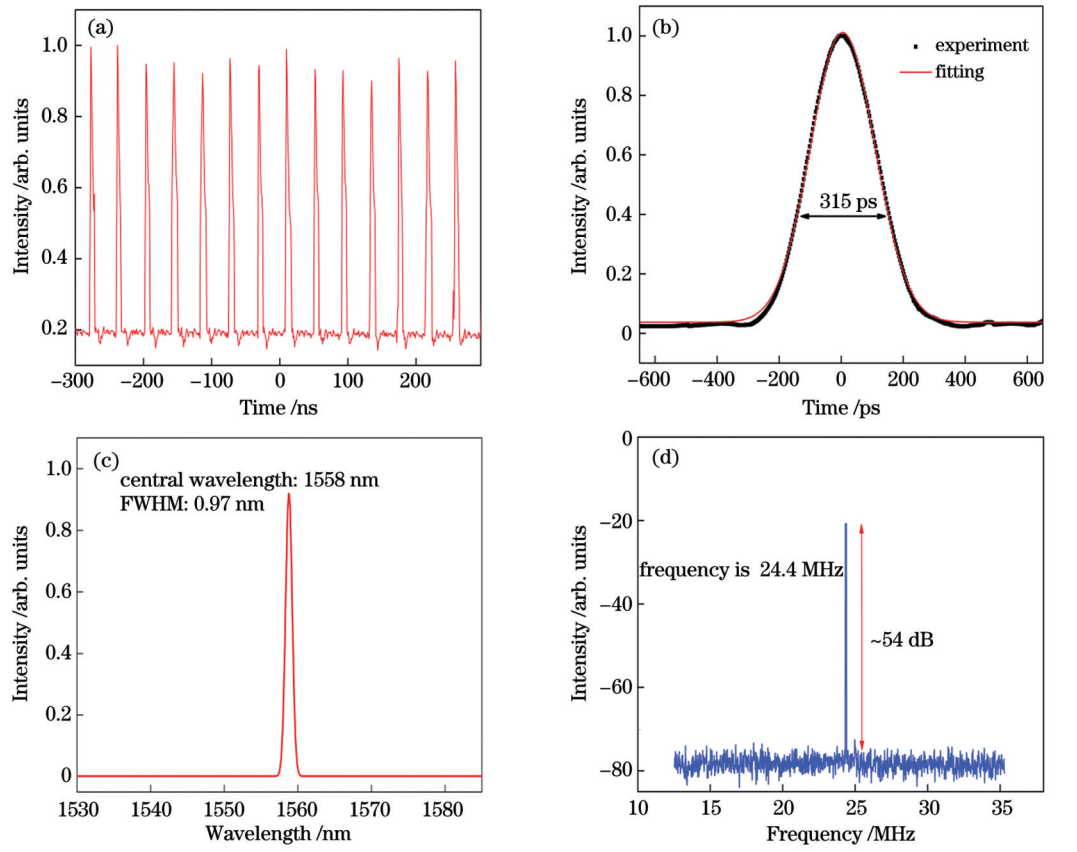

图 7　80 mW 泵浦功率下谐波锁模信号示意图。(a)二次谐波锁模脉冲序列图;(b)自相关曲线图;(c)光谱图;(d)频谱图

Fig. 7　Schematic diagram of harmonic mode-locked signal under 80 mW pump power. (a) Second harmonic mode-locked pulse sequence diagram; (b) autocorrelation curve chart; (c) spectral chart; (d) frequency spectrum

烯器件的响应速度不足以支撑载流子的迁移时间，导致其调制深度发生变化[27]，这也是导致脉冲宽度较宽的原因，脉冲宽度为 315 ps，如图 7(b)所示。图 7(c)、(d)显示了谐波锁模的光谱和频谱信号，光谱的中心波长仍在 1558 nm，但倍频振荡过程会导致多个谐波成分相叠加，进而导致光谱展宽，FWHM 为 0.97 nm。频谱数据显示了谐波锁模信号的频率为 24.4 MHz，对应于激光腔两倍的共振频率，信噪比约为 54 dB。

表 1 列举了使用各类调制技术实现激光器主动锁模的性能参数，从表中可以看出本文所设计的 GCD 调制器能够以较低的功率产生较窄的锁模脉冲，所设计的调制器体积小、制备工艺简单，易于与激光腔集成，且无需复杂的光路设计。通过进一步优化器件参数，完善腔内的色散补偿，可实现性能更优异的主动锁模激光器。

表 1 基于各类调制技术的锁模激光器的参数对比

Table 1 Comparison of parameters of mode-locked lasers based on various modulation techniques

Mode-locking technology	Pump power /mW	Center wavelength /nm	Repetitive frequency /MHz	Pulse width /ps	Reference
Graphene device	80	1558	12.2	298	Our work
Piezoelectric transducer and Bi_2Te_3 topological insulator	50.3	1559.4	5.5	266	Ref. [28]
$LiNbO_3$ Mach-Zehnder modulator	324	1547	12.06	200	Ref. [29]
Acousto-optic modulator	130	1534.45	1.538	330	Ref. [30]
α-$BaTeMo_2O_9$-based acoustooptical modulator	450	1530	3.19	11320	Ref. [31]

4 结 论

本文介绍了一种基于石墨烯全光纤电容型器件的主动锁模光纤激光器，该器件将侧面腐蚀的单模光纤与石墨烯电容型结构相结合，利用光纤倏逝波耦合效应与石墨烯的相互作用，提高了激光的调制效率。此外，基于石墨烯本身的高载流子迁移率和优异的电光特性，在较低调制功耗下实现了激光腔损耗的高速调控，获得了基频和二次谐波的激光锁模运转。实验结果表明，在±5 V的调制信号下，光纤激光器在80 mW的固定泵浦功率下实现了可控重复频率的锁模脉冲，分别为12.2 MHz和24.4 MHz，对应的锁模脉宽分别为298 ps和315 ps，激光中心波长为1558 nm。同时，激光器的平均输出功率随着交流信号幅值的变化可在1.328～1.130 mW范围内调节。本文设计的石墨烯全光纤锁模器件具有低成本、低功耗、占地面积较小和调制频率较高的优势，对实现低功耗、集成化的主动锁模激光器具有重要的参考价值。

参 考 文 献

[1] 谢芷璇, 邓樑旭, 倪溢棉, 等. 波长可调谐和异步双波长锁模掺铒光纤激光器[J]. 光学学报, 2023, 43(4): 0414002.
Xie Z X, Deng L X, Ni Y M, et al. Wavelength-tunable and asynchronous dual-wavelength mode-locked Er-doped fiber laser [J]. Acta Optica Sinica, 2023, 43(4): 0414002.

[2] Han Y, Guo Y B, Gao B, et al. Generation, optimization, and application of ultrashort femtosecond pulse in mode-locked fiber lasers[J]. Progress in Quantum Electronics, 2020, 71: 100264.

[3] Liu J S, Li X H, Guo Y X, et al. $SnSe_2$ nanosheets for subpicosecond harmonic mode-locked pulse generation[J]. Small, 2019, 15(38): 1902811.

[4] Sotor J, Pawliszewska M, Sobon G, et al. All-fiber Ho-doped mode-locked oscillator based on a graphene saturable absorber [J]. Optics Letters, 2016, 41(11): 2592-2595.

[5] 韩冬冬, 张佳月, 高琼, 等. 可切换多波长全光纤被动锁模光纤激光器[J]. 光学学报, 2021, 41(5): 0506002.
Han D D, Zhang J Y, Gao Q, et al. Switchable multi-wavelength passively mode-locked all-fiber lasers[J]. Acta Optica Sinica, 2021, 41(5): 0506002.

[6] Yang B, Zhao H Y, Cao Z Z, et al. Active mode-locking optoelectronic oscillator[J]. Optics Express, 2020, 28(22): 33220-33227.

[7] 胡梁, 钱勇, 李培丽, 等. 基于声光调制模式切换的宽重复频率微秒脉冲光纤放大器[J]. 中国激光, 2023, 50(14): 1401003.
Hu L, Qian Y, Li P L, et al. Wide repetition frequency microsecond pulsed fiber amplifier based on acousto-optic modulating mode switching[J]. Chinese Journal of Lasers, 2023, 50(14): 1401003.

[8] Xia Y Y, Wang J, Zhang Y B, et al. Transmission-type optical modulator based on graphene plasmonic resonator integrated with off-resonant Au structure[J]. Advanced Optical Materials, 2020, 8(18): 2000264.

[9] Shu H W, Jin M, Tao Y S, et al. Graphene-based silicon modulators[J]. Frontiers of Information Technology & Electronic Engineering. 2019, 20(4): 458-471.

[10] Dalir H, Xia Y, Wang Y, et al. Athermal broadband graphene optical modulator with 35 GHz speed[J]. ACS Photonics, 2016, 3(9): 1564-1568.

[11] Kovalchuk O, Uddin S, Lee S, et al. Graphene capacitor-based electrical switching of mode-locking in all-fiberized femtosecond lasers[J]. ACS Applied Materials & Interfaces, 2020, 12(48): 54005-54011.

[12] Dai T F, Chang J H, Deng Z L, et al. Effective switching of an all-solid-state mode-locked laser by a graphene modulator[J]. Optics Express, 2022, 30(10): 16530-16540.

[13] Bogusławski J, Wang Y D, Xue H, et al. Graphene actively mode-locked lasers[J]. Advanced Functional Materials, 2018, 28 (28): 1801539.

[14] Li Y J, Gao L, Zhu T, et al. Graphene-assisted all-fiber optical-controllable laser[J]. IEEE Journal of Selected Topics in Quantum Electronics, 2018, 24(3): 0901709.

[15] Ahmad H, Reduan S A, Yusoff N, et al. Mode-locked pulse generation in erbium-doped fiber laser by evanescent field interaction with reduced graphene oxide-titanium dioxide nanohybrid[J]. Optics & Laser Technology, 2019, 118: 93-101.

[16] Chen Z D, Wang Y G, Li L, et al. Reduced graphene oxide as saturable absorbers for erbium-doped passively mode-locked fiber laser[J]. Chinese Physics B, 2018, 27(8): 084206.

[17] You X, Feng Q, Yang J S, et al. Preparation of high concentration graphene dispersion with low boiling point solvents [J]. Journal of Nanoparticle Research, 2019, 21(1): 19.

[18] Sotor J, Pasternak I, Krajewska A, et al. Sub-90 fs a stretched-pulse mode-locked fiber laser based on a graphene saturable absorber[J]. Optics Express, 2015, 23(21): 27503-27508.

[19] Nair R R, Blake P, Grigorenko A N, et al. Fine structure constant defines visual transparency of graphene[J]. Science, 2008, 320(5881): 1308.

[20] Xu C, Jin Y C, Yang L Z, et al. Characteristics of electro-refractive modulating based on graphene-oxide-silicon waveguide [J]. Optics Express, 2012, 20(20): 22398-22405.

[21] Peng X L, Hao R, Ye Z W, et al. Highly efficient graphene-on-gap modulator by employing the hybrid plasmonic effect[J]. Optics Letters, 2017, 42(9): 1736-1739.

[22] Liu H H, Li Z L, Yu Y, et al. Nonlinear optical properties of anisotropic two-dimensional layered materials for ultrafast photonics[J]. Nanophotonics, 2020, 9(7): 573.

[23] Gene J, Park N H, Jeong H, et al. Optically controlled in-line graphene saturable absorber for the manipulation of pulsed fiber laser operation[J]. Optics Express, 2016, 24(19): 21301-21307.
[24] Yi L J, Li C H. Enhanced absorption and electrical modulation of graphene based on the parity-time symmetry optical structure [J]. Chinese Optics Letters, 2022, 20(2): 022201.
[25] Rodriguez F J, Aznakayeva D E, Marshall O P, et al. Solid-state electrolyte-gated graphene in optical modulators[J]. Advanced Materials, 2017, 29(19): 1606372.
[26] Wang R Y, Jin L, Wang J Z, et al. Harmonic mode-locked fiber laser based on microfiber-assisted nonlinear multimode interference[J]. Chinese Optics Letters, 2022, 20(1): 010601.
[27] Lian T H, Yang K D, Wang X B, et al. Electro-absorption optical modulator based on graphene-buried polymer waveguides [J]. IEEE Photonics Journal, 2020, 12(4): 6601610.
[28] Koo J, Lee J S, Lee J H. Integrated fiber-optic device based on a combination of a piezoelectric transducer and a bulk-structured Bi_2Te_3 topological insulator for *Q*-switched mode-locking of a fiber laser[J]. Journal of Lightwave Technology, 2017, 35(11): 2175-2182.
[29] Zhou Y, Wang A T, Gu C, et al. Actively mode-locked all fiber laser with cylindrical vector beam output[J]. Optics Letters, 2016, 41(3): 548-550.
[30] Cuadrado-Laborde C, Bello-Jiménez M, Díez A, et al. Long-cavity all-fiber ring laser actively mode locked with an in-fiber bandpass acousto-optic modulator[J]. Optics Letters, 2013, 39 (1): 68-71.
[31] Xu Q, Liu F A, Gao Z L, et al. Actively *Q*-switched and mode-locked all-fiber lasers with an α-$BaTeMo_2O_9$-based acousto-optical modulator[J]. Applied Optics, 2021, 60(35): 10838-10842.

All-Fiber Actively Mode-Locked Laser Based on Graphene

Su Youpeng[1,2], Chang Jianhua[1,2,3*], Lu Tianyi[1,2], Cui Zhiyuan[1,2], Tu Qian[1,2], Zhu Yunhan[1,2]

[1]*TianChang Research Institute, Nanjing University of Information Science & Technology, Chuzhou* 239300, *Anhui, China*;

[2]*School of Electronics & Information Engineering, Nanjing University of Information Science and Technology, Nanjing* 210044, *Jiangsu, China*;

[3]*Collaborative Innovation Center of Atmospheric Environment and Equipment Technology, Nanjing University of Information Science and Technology, Nanjing* 210044, *Jiangsu, China*

Abstract

Objective Ultra-fast pulse fiber lasers are extensively employed in fields such as fiber optic communication, medicine, and precision material processing due to their compact structure and high beam quality. Lock mode technology is an effective method for achieving ultra-short pulses. Actively mode-locked lasers introduce active modulation devices into the laser cavity and adopt external modulation signals to change the optical signal characteristics, achieving a laser mode-locked pulse output. They feature flexibility, controllability, and stable output pulses. In recent years, graphene has been extensively studied due to its excellent electro-optical properties. Research has shown that an external electric field can alter the Fermi level of graphene to achieve light absorption modulation. Therefore, graphene-based electro-optic modulators have the potential to achieve actively mode-locked lasers. We present the construction of an efficient and high-speed graphene all-fiber mode-locked device, which achieves high-speed adjustment of graphene′s optical performance with low modulation power consumption and high modulation efficiency.

Methods The device is composed of graphene, single-mode optical fiber, polydimethylsiloxane (PDMS), and silver (Ag) film, forming a capacitive device (GCD) structure. By selecting glass as the substrate and leveraging magnetron sputtering technology to deposit 50 nm silver on the glass as the bottom electrode, silver has sound conductivity, which is beneficial for reducing the device resistance. The insulation layer is a spin-coated 200 nm PDMS layer, and the thinner insulation layer can effectively reduce the capacitance value of the device. Meanwhile, hydrofluoric acid (HF) with a concentration of 20% is utilized to corrode standard single-mode optical fibers to 15 μm with a corrosion length of 5 mm, and the corroded single-mode fiber is transferred to PDMS. The device is placed in a UV ozone cleaning machine (multi-frequency, CCI UV250-MC) for 10 minutes to improve the hydrophilicity of the insulation layer PDMS. There is graphene dispersion with a selected concentration of 0.1 mg/mL (Nanjing Xianfeng Nanomaterial Technology Co., Ltd., XFZ20 dispersion). Graphene solution is dropped onto the optical fiber, dried, and then inkjet printed with a silver electrode layer on the device using a microelectronic printer (Power Supply Technology Co., Ltd., MP1100). Finally, the prepared device is connected to the circuit board using silver wire. The GCD device is connected between the isolator and polarization controller by fusion, and a spectrum analyzer, digital oscilloscope, power meter, autocorrelator, and spectrum analyzer are adopted to

record the locked pulse signal, including spectrum, pulse width, repetition rate, and output power.

Results and Discussions The GCD device is connected to the fiber laser system and a pump power of 80 mW is employed for actively mode-locked experiments. At a pump power of 80 mW, the AC signal amplitude increases from 0 V to 5 V, and the average output power decreases from 1.328 mW to 1.130 mW. After calculation, the insertion loss of the device increases from 1.54 dB to 2.46 dB (Fig. 4). Subsequently, a periodic AC signal (12.2 MHz) that is consistent with the resonant frequency of the laser cavity is applied to the graphene device. Under low voltage amplitude, the control of the graphene Fermi level is limited, resulting in a limited range of dynamic changes in the absorption of graphene devices. Therefore, unstable mode-locked pulse signals are observed. When the voltage amplitude increases to 5 V, the most stable mode-locked pulse signal is observed to achieve active mode locking of the laser. The narrowest pulse width of the mode locking signal is 298 ps (Fig. 5). Meanwhile, by increasing the modulation frequency to twice the resonant frequency of the laser cavity (24.4 MHz), the optical signal inside the cavity undergoes frequency doubling oscillation under the graphene device control, leading to harmonic mode-locked operation. The mode-locked pulse signal is slightly unstable, possibly due to the insufficient response speed of graphene to support the migration time of charge carriers at higher modulation rates, resulting in modulation depth changes in the device. This is also the reason for the wider pulse width of 315 ps, corresponding to a frequency of 24.4 MHz, which achieves active repetition frequency control in mode-locked lasers.

Conclusions We introduce an actively mode-locked fiber laser based on a graphene all-fiber structure. It combines single-mode optical fibers that have undergone lateral corrosion treatment with graphene capacitor structures and utilize the evanescent wave coupling effect of optical fibers to interact with graphene, achieving efficient modulation. Meanwhile, by utilizing the inherent high carrier mobility of graphene, high-speed adjustment of optical performance can be achieved with lower modulation power consumption. The experimental results show that under a modulation signal of $\pm$5 V, the fiber laser obtains controllable repetitive mode-locked pulses at a fixed pump power of 80 mW, with frequencies of 12.2 MHz and 24.4 MHz respectively. The corresponding mode-locked pulse widths are 298 ps and 315 ps respectively, and the laser center wavelength is 1558 nm. Meanwhile, by changing the amplitude of the AC signal (0–5 V), the average output power of the laser can be adjusted within the range of 1.328 mW to 1.130 mW. The research results provide references for achieving low-power and integrated actively mode-locked lasers, and have practical significance for developing efficient and integrated actively mode-locked laser systems.

Key words lasers; fiber laser; graphene; all-fiber structure; active mode-locking